

High-density liquid (HDL) adsorption at the supercooled water/vapor interface and its possible relation to the second surface tension inflection point

Alexander Gorfer,¹ Christoph Dellago,^{1,2} and Marcello Sega³

¹*Faculty of Physics, University of Vienna, Boltzmannngasse 5, Wien A-1090, Austria*

²*Erwin Schrödinger Institute for Mathematics and Physics, Boltzmannngasse 9, 1090, Vienna, Austria*

³*Department of Chemical Engineering, University College London, London WC1E 7JE, United Kingdom*

(*Electronic mail: m.sega@ucl.ac.uk)

(Dated: 17 November 2022)

We investigate the properties of water along the liquid/vapor coexistence line in the supercooled regime down to the no-man’s land. Extensive molecular dynamics simulations of the TIP4P/2005 liquid/vapor interface in the range 198 – 348 K allow us to locate the second surface tension inflection point with high accuracy at 283 ± 5 K, close to the temperature of maximum density (TMD). This temperature also coincides with the appearance of a density anomaly at the interface known as the apophysis. We relate the emergence of the apophysis to the observation of HDL water adsorption in the proximity of the liquid/vapor interface.

I. INTRODUCTION

The rich set of anomalous properties of water has kept it an active area of research, in particular regarding the thermodynamic and kinetic properties of the supercooled liquid state. These properties are governing the freezing of water^{1,2} and are key in diverse fields like climatology^{3,4} or cryobiology^{5,6}, but experiments aimed at investigating the properties in the deeply supercooled region face an almost insurmountable challenge. Below the temperature of homogenous nucleation T_H , frequently reported to be around 235 K⁷, water freezes faster than the time it takes to measure response functions. Therefore, most measurements become impossible. The region of temperatures below T_H has been named the no-man’s land, and the properties of water in this region have become topics of intense debate⁸.

One of the subjects of debate is the source of the drastic evolution of water’s response functions in the supercooled regime. A popular explanation involves the presence of a liquid-liquid first order phase transition⁹ between high-density (HDL) and ice-like low-density liquid (LDL) water upon lowering the temperature. In this scenario, the associated critical point explains the divergent behavior of water’s response functions inside the no-man’s land.

A second debated topic is the presence of a second, low-temperature inflection point of the surface tension as a function of temperature. Above the melting point, the surface tension of water follows with high accuracy the empirical equation of the International Association for the Properties of Water and Steam (IAPWS)^{10,11}

$$\gamma = B \left(\frac{T_c - T}{T_c} \right)^\mu \left(1 + b \frac{T_c - T}{T_c} \right), \quad (1)$$

where $T_c = 647.096$ K is the critical temperature and the remaining parameters are $B = 235.8$ mN/m, $b = -0.625$ and $\mu = 1.256$. The IAPWS curve agrees with measured data well below the melting point¹². However, whether this agree-

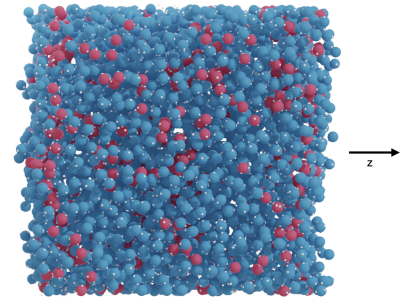


FIG. 1. Simulation snapshot taken at 198.15 K, showing HDL (red oxygen atoms) and LDL (blue oxygen atoms) molecules, where the accumulation of HDL molecules close to the liquid/vapor interface is evident by simple visual inspection. The surface normal points along z .

ment can continue deeper in the supercooled regime is controversial, as measurements of surface tension become very involved¹³. A recent experimental study¹⁴ measured the surface tension of water down to about 241 K using the capillary rise method and reported a deviation from the IAPWS equation that opens the possibility of the existence of a second inflection point. Computational studies support the appearance of the second inflection point for several water models, including SPC/E^{15,16}, TIP4P/2005¹⁶ and WAIL¹⁷.

Simulations of explicit liquid/vapor coexistence of supercooled water have also exhibited a compact layer at the water/vapor interface that manifests itself as a shoulder in the density profiles^{16,18–22}. Wang and coworkers¹⁶ suggested a connection of this feature to the second inflection point of the surface tension. Still, a systematic study of this anomaly and its links to other anomalous features has not been attempted so far. The outermost layer of the water/vapor interface is known to have a significantly different structure^{23–25} than the bulk liquid. However, a systematic analysis of the properties

of water layers in the supercooled regime is missing, particularly taking care of analyzing the distribution of HDL and LDL water, which is supposed to be of particular relevance in the no-man’s land.

Here, we use extensive molecular dynamics simulations of water in the supercooled regime to investigate the region around the surface tension’s second inflection point with high accuracy. We characterize the local composition of the two liquid phases as a function of the proximity to the outermost molecular layer. We find that the second inflection point lies at the somewhat unexpectedly high temperature of 280 K, in correspondence with the appearance of a shoulder in the density profile and the TMD. While the presence of the shoulder could be partly explained by the reduced amplitude of thermal capillary waves, we observe the concurrent preference of HDL water to accumulate at the liquid/vapor interface. The larger freedom to perform structural reorganization at the liquid/vapor interface justifies the increased concentration of HDL water. Its larger entropy could be the origin of the increased surface tension in the no-man’s land.

II. METHODS

Our water model of choice is the TIP4P/2005 one²⁶, which reproduces the phase diagram of water with high accuracy. The TIP4P/2005 model shows the presence of the liquid-liquid phase transition^{27–30}, and two-state equations of state well explain its thermodynamic properties^{31,32}. Recently, Wang and coworkers¹⁶ showed that the TIP4P/2005 model is compatible with the presence of a surface tension second inflection point, a feature accompanied by the appearance of a density shoulder (apophysis) in the supercooled regime.

We performed molecular dynamics simulations of water in the slab configuration using the GROMACS 2019.3³³ simulation package. We started from a cubic simulation box with periodic boundary conditions measuring $5 \times 5 \times 5 \text{ nm}^3$ filled with 4017 water molecules. We kept the molecular structure rigid using the SETTLE³⁴ algorithm and integrated the equations of motion using the leapfrog algorithm with a timestep of 1 fs. We computed the long-range contribution of dispersion and Coulomb interactions using the smooth version of the Particle Mesh Ewald algorithm^{35,36}. We employed a real-space cutoff of 1.3 nm and a relative interaction strength at the cutoff of 10^{-3} and 10^{-5} for the Lennard-Jones and Coulomb interactions, respectively, and a grid spacing of 0.15 nm. We used the Nosé–Hoover thermostat^{37,38} with a time constant of 2 ps for both the equilibration and production runs.

First, we equilibrated for 10 ns 19 copies of the system at the target temperature values ranging from 198.15 to 348.15 K. After this initial phase, we extended the z box edge to 20 nm to obtain the liquid/vapor interface in slab configuration, as depicted in Fig. 1. Subsequently, we performed an additional equilibration phase reaching up to 80 ns for the lowest temperature. During the production runs, which lasted up to 250 ns for the lowest temperature, we saved to disk for further analysis the configurations every 1 ps and energy and pressure every 0.1 ps. In total, we simulated more than 9.5 μs .

The reader can find the details of equilibration and production runs in the Supplemental Information.

We analyzed the stored configurations for structural features, including profiles across the liquid slab of density, number of neighbors and HDL fraction. Our analysis made extensive use of the Pytim package³⁹ which expands upon MD-Analysis^{40,41}. We computed the profiles of the quantities of interest across the slab using 0.2 nm wide bins. Additionally, we singled out the contributions of the first four interfacial layers⁴² using the Identification of Truly Interfacial Molecules (ITIM) algorithm²³ as implemented in Pytim, using a probe-sphere radius of 0.15 nm. We considered two molecules neighbors if the distance between the respective oxygen atoms is less than $r_S = 0.35 \text{ nm}$. This distance encompasses the first oxygen coordination shell reasonably well over a broad temperature range. To classify a molecule as HDL or LDL, we employed the fifth neighbor criterion (d_5)⁴³ that categorizes molecules whose fifth neighbor lies farther away than r_S as LDL ones and as HDL ones otherwise. Using the stored values of the pressure tensor, we calculated the surface tension γ using the mechanical definition

$$\gamma = \frac{L_z}{2} \left[\langle P_z \rangle - \frac{\langle P_x \rangle + \langle P_y \rangle}{2} \right], \quad (2)$$

where $L_z = 20 \text{ nm}$ is the length of the box edge that is perpendicular to the macroscopic interface and $\langle P_\alpha \rangle$ is the diagonal component of the pressure tensor in direction α , averaged in the canonical ensemble (angular brackets) over the complete production run.

III. RESULTS AND DISCUSSION

To investigate the presence of the second inflection point of $\gamma(T)$ we considered (a) the departure of $\gamma(T)$ from a fit to the IAPWS equation, (b) a fit to a Fermi function, and (c) the calculation of the surface excess entropy using finite differences. To show the departure from the IAPWS values, we first adjusted the parameters of the IAPWS equation to the TIP4P/2005 model by fitting Eq.(1) to the measured $\gamma(T)$ above the melting point, keeping only the exponent μ fixed at 11/9. The result of the optimization are $B = 206.2 \text{ mN/m}$, $b = -0.557$ and a critical temperature T_c of 661.543 K. The surface tension data and the IAPWS extrapolation below the melting point is shown in Fig. 2, where we also report the simulation data of Wang and coworkers¹⁶ and the experimental points from Ref.¹⁴, for comparison. The departure from the IAPWS equation shows the presence of an anomalous rise of the surface tension at low temperatures, implying the presence of an inflection point.

To locate the inflection point accurately, we perform the best fit of our simulation data $T(\gamma)$ to an inverted Fermi function,

$$T(\gamma) = \frac{C}{1 - e^{D(\gamma - \gamma_0)}} + E, \quad (3)$$

with C, D, E and γ_0 fitting parameters. This function has no particular physical significance, and it is used only as an effi-

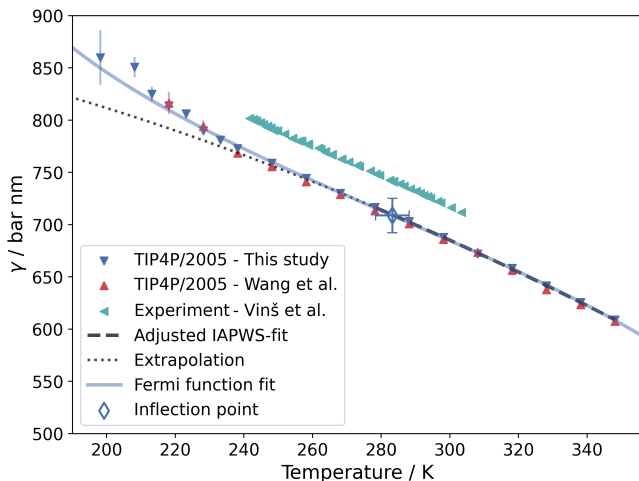


FIG. 2. Surface tension as a function of temperature for this study, Wang et al., Ref. 16 and for Vinš et al., Ref. 14.

cient way to extract the inflection point²⁴. Additionally, following Wang and coworkers¹⁶, we also calculated the surface excess entropy per unit area⁴⁴ $s_x = -d\gamma/dT$ to locate the inflection point as the minimum of s_x . To compute $d\gamma/dT$ we applied the method of central differences to the sampled values of γ . Our data are compatible with those of Wang and coworkers¹⁶. Still, the larger set of temperatures and longer sampling times allow the determination of the inflection point with higher accuracy. The best fit of the Fermi function yields an inflection temperature of 283 ± 5 K. This value is in agreement with the minimum of s_x , located at 278.15 K (see SI) and is very close to the TMD (about 280 K). If we exclude the points below 223.15 K (based on possible concerns on the ergodicity of the sampled data, discussed further on), the best fit yields an inflection temperature of 275 ± 12 K, still compatible with the estimate that uses the whole dataset.

Applying the Fermi function fit procedure to the experimental data of Vinš and coworkers leads to an estimate of the inflection point temperature of 267 ± 2 K.

Next, we investigate the possible relation of the local structure with the thermodynamics of the second inflection point in terms of density, the number of neighbors, and the fraction of HDL (or LDL) water.

Figure 3 shows the number density profile of the whole slab and those of the first four layers on each of its two sides. A small dot marks the location of the density maximum in each layer. We notice that for the lowest 2-3 temperature values, the density profiles are not uniform far from the surface, showing signs of what seems to be insufficient sampling, despite averaging over long trajectories (250 ns for the lowest temperature). Obviously, for the lowest 2-3 temperatures, the systems show the signature of being in a glassy, non-ergodic state. However, close to the interface, the density profile appears smoother and well converged even at the lowest temperature. We will come back to this point later in our analysis. For the time being, we concentrate on the emergence of the density maximum close to the surface, which is not affected

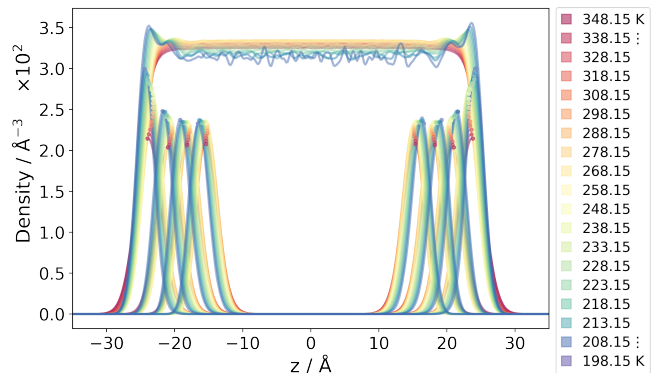


FIG. 3. Molecular number density profiles of the whole system and the first four layers. Dots signify layers' center of mass.

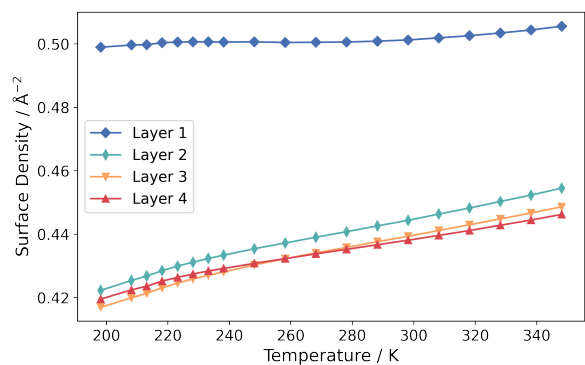


FIG. 4. Integrated density profiles of the layers.

by ergodicity issues.

The density maximum at the interface is the so-called apophysis reported in several studies^{16,18–21,45}. The apophysis appears close to the maximum of the first molecular layer. Next to the apophysis, it is possible to spot a weaker but still well-defined second peak located in the proximity of the second molecular layer. One could legitimately question whether the apophysis is only the result of the diminished amplitude of thermal capillary waves. A density profile is, in fact, a correlation function in disguise, where the local density is correlated with the location of the center of mass of the slab. Upon cooling, the smearing effect of capillary waves diminishes, and the correlation due to molecular layering can appear. Wang and coworkers¹⁶ performed a finite size study using boxes with a transverse size L of 5 and 10 nm and showed that the apophysis does not disappear when simulating the wider box. However, one needs to consider that at those low temperatures the width of the interface superimposed by thermal capillary fluctuations as predicted by the capillary wave theory⁴⁶ is still smaller than the molecular size of water (0.35 nm) even for $L = 10$ nm. In this sense, we could expect that capillary wave fluctuations cannot smear the apophysis even in the larger simulation box considered in Ref.¹⁶.

Despite this, the analysis of the molecular layers shows that the peak density of the first layer behaves quite differ-

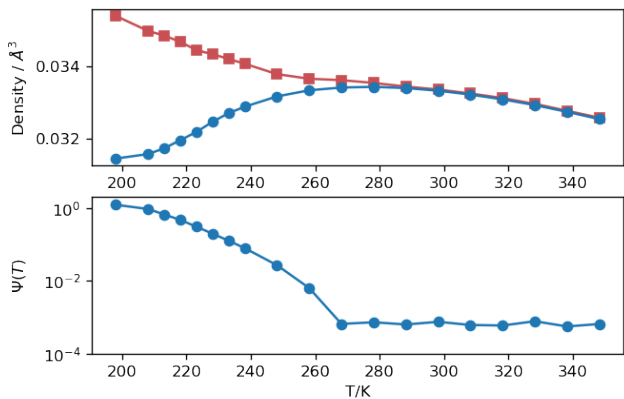


FIG. 5. Top panel: Maximum of the density profile (red squares) and density in the middle of the slab (blue circles), as a function of temperature. Bottom panel: HDL peak order parameter Ψ of the HDL fraction as a function of temperature.

ently from the subsequent ones, as its value keeps growing at a much stronger rate than the subsequent ones. When the temperature decreases, the distribution of molecules in layers changes not only in height but also in width. Integrating these distributions yields the number of molecules in each layer, which we report as surface density in Fig. 4. The first layer stands out not only because of its more (laterally) densely packed structure but also because of its temperature-insensitive nature. As the layer surface density reported in Fig. 4 is an intrinsic property, it shows that the apophysis (or at least part of it) is not an artifact of capillary fluctuations. This confirms by other means and for planar interfaces the result obtained by Malek, Poole and Saika-Voivod for water nanodroplets²², who employed the Voronoi tessellation to compute the local density and avoid the spurious layering.

A comparison of the density value at its maximum and in bulk, as reported in Fig. 5, shows that also the apophysis starts emerging at about 280 K, roughly the same temperature as that of the inflection temperature and of the TMD. The existence of the TMD in water can be explained by the thermodynamic competition between LDL and HDL water^{9,47,48}, with LDL water becoming increasingly more likely than HDL when the temperature decreases. Therefore, it makes sense to investigate the water slab composition in terms of LDL and HDL fractions as a function of the proximity to the interfacial layer.

Using the fifth neighbor criterion, we compute the profile of HDL water's fraction $f(z)$ along the surface normal. Close to the vapor phase, a growing number of molecules belonging to the first layer contribute to the histogram, and the definition of HDL fraction ceases to be meaningful. Surface layer molecules necessarily have fewer neighbors than molecules in the subsequent layers, so the HDL fraction profile drops to zero. As long as a complete shell of neighbors surrounds a molecule, starting from molecules belonging to the second layer, the value of the computed HDL fraction is meaningful. The profiles of the HDL fraction reported in Fig. 6 show the fascinating appearance of an accumulation of HDL water

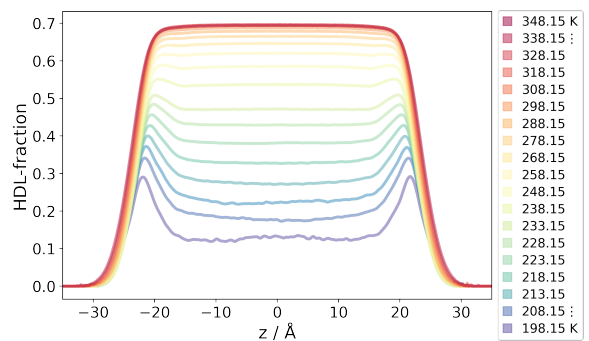


FIG. 6. Profiles of the fraction of HDL across the system.

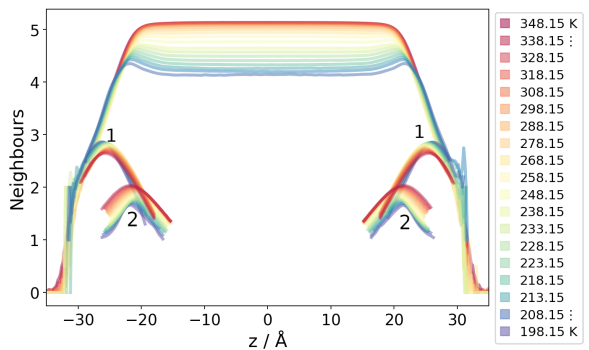


FIG. 7. Profiles of the number of neighbors for the whole system and of the number of intra-layer neighbors for layers 1 and 2.

at the surface upon lowering the temperature. In the surface layer, the fifth neighbor criterion cannot be used anymore, and the fraction of HDL drops to zero close to the interface. However, taking into account the fact that first layer molecules are the most densely packed (Fig. 4), the emerging picture is that of a positive excess density of HDL (beyond the first layer) and HDL-like molecules (in the first layer).

To formalize the onset of the positive excess density of HDL, we compute an order parameter Ψ , shown in the bottom panel of Fig. 5 from the HDL fraction value at its maximum f_{\max} and in the bulk f_{bulk} as

$$\Psi(T) = f_{\max}(T)/f_{\text{bulk}}(T) - 1. \quad (4)$$

The order parameter is constant and close to zero at high temperature until about 270 K, when it increases upon decreasing the temperature. This behavior is similar to that of a second order phase transition, once again in the neighborhood of the TMD.

It is also interesting to observe the average number of neighbors (regardless of the layer they belong to) as a function of temperature and position along the slab and the number of intra-layer neighbors for the first two layers. We report these profiles in Fig. 7. In the central region, the average number of neighbors decreases from about five at the highest temperature to slightly more than four at the lowest. This behavior underlines the change from the preponderance of HDL

to that of LDL upon entering the supercooled regime. Peaks in the number of neighbors for the whole system develop at low temperatures, reflecting the presence of a positive HDL surface excess. The distributions of the intra-layer neighbors show that the second layer has about two intra-layer neighbors at high temperatures, most likely corresponding to two in-layer hydrogen bonds (the other two connecting atoms being in the first and third layers). At lower temperatures, the number of intra-layer neighbors decreases systematically. The first layer shows the opposite behavior, as the number of intra-layer neighbors increases upon cooling. This result confirms the picture of a more compact first layer shown in Fig. 4. It is somehow intuitive that the possibility for molecules in the first layer to coordinate more neighbors (overall and within the same layer) is related to the larger freedom they enjoy because they do not need to fit the tetrahedral structure imposed by the hydrogen bond network in the bulk. As the system is cooled, bulk water molecules transition from HDL to LDL, lowering their configurational entropy. This transition does not happen close to the surface, where access to the less constrained first layer allows to keep a higher packing and a (relatively to the bulk) higher HDL concentration. The overall effect is an increased surface excess entropy and the consequent larger negative slope of the surface tension.

IV. CONCLUSIONS

Using extensive molecular dynamics simulations of water along the coexistence line, we confirm and provide robust evidence of the presence of a second inflection point of its surface tension at low temperature, in connection with an increased interfacial adsorption of high density liquid water. The high accuracy of our sampling allows locating the inflection point at a higher temperature than previously suggested. The temperature of the inflection point, as estimated from the surface tension fit (283 ± 5 K) and from its numerical differentiation (278 ± 5 K) is compatible with the TMD along the coexistence line (278 ± 5 K). The inflection of the surface tension and its corresponding positive deviation from the fit to the IAWPS equation upon cooling correlates strongly with the appearance of a shoulder in the density profile at the liquid-vapor interface, known as the apophysis. We showed that the presence of this shoulder is not an artifact of the narrower capillary wave fluctuations at low temperatures but is indeed the result of a more compact surface layer. This compact layer is allowed to form thanks to the larger configurational entropy enjoyed by molecules in the surface layer. However, the increase in local density is not limited to the first molecular layer, as the distribution of HDL water molecules across the water slab shows. While the composition of the water slab becomes richer in LDL water, there is a clear accumulation of HDL water close to the interface when the temperature decreases. The order parameter of the HDL fraction suggests a mechanism similar to a second order phase transition, with the equivalent of a critical point located at 268 ± 5 K, also in proximity of the TMD.

SUPPLEMENTARY MATERIAL

Additional information on the simulations and plots of surface excess entropy, number of neighbors and their profiles as a function of temperature, and peak density, HDL fraction and surface tension correlation plots.

ACKNOWLEDGMENTS

We acknowledge financial support of the Austrian Science Fund (FWF) through grant number I 4404. The computational results presented have been achieved using the Vienna Scientific Cluster (VSC).

- ¹R. A. Nistor, T. E. Markland, and B. J. Berne, "Interface-Limited Growth of Heterogeneously Nucleated Ice in Supercooled Water," *J. Phys. Chem. B* **118**, 752–760 (2014).
- ²M. Fitzner, G. C. Sosso, S. J. Cox, and A. Michaelides, "Ice is born in low-mobility regions of supercooled liquid water," *Proc. Natl. Acad. Sci. U.S.A.* **116**, 2009–2014 (2019).
- ³Y. Hu, S. Rodier, K.-m. Xu, W. Sun, J. Huang, B. Lin, P. Zhai, and D. Josset, "Occurrence, liquid water content, and fraction of supercooled water clouds from combined CALIOP/IIR/MODIS measurements," *J. Geophys. Res.-Atmos.* **115**, D00H34 (2010).
- ⁴B. J. Murray, D. O'Sullivan, J. D. Atkinson, and M. E. Webb, "Ice nucleation by particles immersed in supercooled cloud droplets," *Chem. Soc. Rev.* **41**, 6519 (2012).
- ⁵P. Mazur, "Cryobiology: The Freezing of Biological Systems: The responses of living cells to ice formation are of theoretical interest and practical concern." *Science* **168**, 939–949 (1970).
- ⁶P. Wilson, A. Heneghan, and A. Haymet, "Ice nucleation in nature: Supercooling point (SCP) measurements and the role of heterogeneous nucleation," *Cryobiology* **46**, 88–98 (2003).
- ⁷A. Manka, H. Pathak, S. Tanimura, J. Wölk, R. Strey, and B. E. Wyslouzil, "Freezing water in no-man's land," *Phys. Chem. Chem. Phys.* **14**, 4505–4516 (2012).
- ⁸J. C. Palmer, P. H. Poole, F. Sciortino, and P. G. Debenedetti, "Advances in Computational Studies of the Liquid-Liquid Transition in Water and Water-Like Models," *Chem. Rev.* **118**, 9129–9151 (2018).
- ⁹P. Gallo, K. Amann-Winkel, C. A. Angell, M. A. Anisimov, F. Caupin, C. Chakravarty, E. Lascaris, T. Loerting, A. Z. Panagiotopoulos, J. Russo, J. A. Sellberg, H. E. Stanley, H. Tanaka, C. Vega, L. Xu, and L. G. M. Pettersson, "Water: A Tale of Two Liquids," *Chem. Rev.* **116**, 7463–7500 (2016).
- ¹⁰IAPWS, "Revised release on surface tension of ordinary water substance," *Tech. Rep.* (IAPWS, Moscow, Russia, 2014).
- ¹¹N. B. Vargaftik, B. N. Volkov, and L. D. Voljak, "International tables of the surface tension of water," *J. Phys. Chem. Ref. Data* **12**, 817–820 (1983).
- ¹²J. Hrubý, V. Vinš, R. Mareš, J. Hykl, and J. Kalová, "Surface tension of supercooled water: No inflection point down to -25 °C," *Journal of Physical Chemistry Letters* **5**, 425–428 (2014).
- ¹³V. Vinš, M. Fransen, J. Hykl, and J. Hrubý, "Surface tension of supercooled water determined by using a counterpressure capillary rise method," *J. Phys. Chem. B* **119**, 5567–5575 (2015).
- ¹⁴V. Vinš, J. Hykl, J. Hrubý, A. Blahut, D. Celný, M. Čenský, and O. Prokopová, "Possible anomaly in the surface tension of supercooled water: New experiments at extreme supercooling down to -31.4 °C," *J. Phys. Chem. Lett.* **11**, 4443–4447 (2020).
- ¹⁵Y. J. Lü and B. Wei, "Second inflection point of water surface tension," *Appl. Phys. Lett.* **89**, 164106 (2006).
- ¹⁶X. Wang, K. Binder, C. Chen, T. Koop, U. Pöschl, H. Su, and Y. Cheng, "Second inflection point of water surface tension in the deeply supercooled regime revealed by entropy anomaly and surface structure using molecular dynamics simulations," *Phys. Chem. Chem. Phys.* **21**, 3360–3369 (2019).

- ¹⁷T. R. Rogers, K. Y. Leong, and F. Wang, "Possible evidence for a new form of liquid buried in the surface tension of supercooled water," *Scientific Reports* **6**, 1–6 (2016).
- ¹⁸H. Matsubara, T. Koishi, T. Ebisuzaki, and K. Yasuoka, "Extended study of molecular dynamics simulation of homogeneous vapor-liquid nucleation of water," *J. Chem. Phys.* **127**, 214507 (2007).
- ¹⁹K. Abe, T. Sumi, and K. Koga, "Temperature dependence of local solubility of hydrophobic molecules in the liquid-vapor interface of water," *Journal of Chemical Physics* **141**, 18C516 (2014).
- ²⁰A. Haji-Akbari, R. S. DeFever, S. Sarupria, and P. G. Debenedetti, "Suppression of sub-surface freezing in free-standing thin films of a coarse-grained model of water," *Phys. Chem. Chem. Phys.* **16**, 25916–25927 (2014).
- ²¹A. Haji-Akbari and P. G. Debenedetti, "Computational investigation of surface freezing in a molecular model of water," *Proc. Natl. Acad. Sci. U.S.A.* **114**, 3316–3321 (2017).
- ²²S. M. Malek, P. H. Poole, and I. Saika-Voivod, "Thermodynamic and structural anomalies of water nanodroplets," *Nat. Comm.* **9**, 1–9 (2018).
- ²³L. B. Pártay, G. Hantal, P. Jedlovsky, Á. Vincze, and G. Horvai, "A new method for determining the interfacial molecules and characterizing the surface roughness in computer simulations. Application to the liquid-vapor interface of water," *J. Comput. Chem.* **29**, 945–956 (2008).
- ²⁴M. Sega, G. Horvai, and P. Jedlovsky, "Microscopic origin of the surface tension anomaly of water," *Langmuir* **30**, 2969–2972 (2014).
- ²⁵M. Bonn, Y. Nagata, and E. H. Backus, "Molecular Structure and Dynamics of Water at the Water-Air Interface Studied with Surface-Specific Vibrational Spectroscopy," *Angew. Chem. Int. Ed.* **54**, 5560–5576 (2015).
- ²⁶J. L. Abascal and C. Vega, "A general purpose model for the condensed phases of water: TIP4P/2005," *J. Chem. Phys.* **123**, 234505 (2005).
- ²⁷J. Russo and H. Tanaka, "Understanding water's anomalies with locally favoured structures," *Nat. Comm.* **5**, 1–11 (2014), arXiv:1308.4231.
- ²⁸J. L. Abascal and C. Vega, "Widom line and the liquid-liquid critical point for the TIP4P/2005 water model," *Journal of Chemical Physics* **133**, 234502 (2010).
- ²⁹D. T. Limmer and D. Chandler, "Theory of amorphous ices," *Proc. Natl. Acad. Sci. U.S.A.* **111**, 9413–9418 (2014).
- ³⁰P. H. Handle, T. Loerting, and F. Sciortino, "Supercooled and glassy water: Metastable liquid(s), amorphous solid(s), and a no-man's land," *Proc. Natl. Acad. Sci. U.S.A.* **114**, 13336–13344 (2017).
- ³¹F. Bresme, J. W. Biddle, J. V. Sengers, and M. A. Anisimov, "Communication: Minimum in the thermal conductivity of supercooled water: A computer simulation study," *J. Chem. Phys.* **140**, 161104 (2014).
- ³²R. S. Singh, J. W. Biddle, P. G. Debenedetti, and M. A. Anisimov, "Two-state thermodynamics and the possibility of a liquid-liquid phase transition in supercooled TIP4P/2005 water," *J. Chem. Phys.* **144**, 144504 (2016).
- ³³M. J. Abraham, T. Murtola, R. Schulz, S. Páll, J. C. Smith, B. Hess, and E. Lindah, "Gromacs: High performance molecular simulations through multi-level parallelism from laptops to supercomputers," *SoftwareX* **1–2**, 19–25 (2015).
- ³⁴S. Miyamoto and P. A. Kollman, "Settle: An analytical version of the SHAKE and RATTLE algorithm for rigid water models," *J. Comput. Chem.* **13**, 952–962 (1992).
- ³⁵U. Essmann, L. Perera, M. L. Berkowitz, T. Darden, H. Lee, and L. G. Pedersen, "A smooth particle mesh Ewald method," *J. Chem. Phys.* **103**, 8577–8593 (1995).
- ³⁶M. Sega and C. Dellago, "Long-Range Dispersion Effects on the Water/Vapor Interface Simulated Using the Most Common Models," *J. Phys. Chem. B* **121**, 3798–3803 (2017).
- ³⁷S. Nosé, "A unified formulation of the constant temperature molecular dynamics methods," *J. Chem. Phys.* **81**, 511–519 (1984).
- ³⁸W. G. Hoover, "Canonical dynamics: Equilibrium phase-space distributions," *Phys. Rev. A* **31**, 1695–1697 (1985).
- ³⁹M. Sega, G. Hantal, B. Fábrián, and P. Jedlovsky, "Pytim: A python package for the interfacial analysis of molecular simulations," *J. Comput. Chem.* **39**, 2118–2125 (2018).
- ⁴⁰N. Michaud-Agrawal, E. J. Denning, T. B. Woolf, and O. Beckstein, "MDAnalysis: A toolkit for the analysis of molecular dynamics simulations," *J. Comput. Chem.* **32**, 2319–2327 (2011).
- ⁴¹R. Gowers, M. Linke, J. Barnoud, T. Reddy, M. Melo, S. Seyler, J. Domański, D. Dotson, S. Buchoux, I. Kenney, and O. Beckstein, "MDAnalysis: A python package for the rapid analysis of molecular dynamics simulations," in *Proceedings of the 15th Python in Science Conference (SciPy, 2016)* pp. 98–105.
- ⁴²M. Sega, B. Fábrián, and P. Jedlovsky, "Layer-by-layer and intrinsic analysis of molecular and thermodynamic properties across soft interfaces," *J. Chem. Phys.* **143**, 114709 (2015).
- ⁴³M. J. Cuthbertson and P. H. Poole, "Mixturelike behavior near a liquid-liquid phase transition in simulations of supercooled water," *Phys. Rev. Lett.* **106**, 115706 (2011).
- ⁴⁴J. S. Rowlinson and B. Widom, *Molecular Theory of Capillarity* (Dover Publications, Inc., Mineola, New York, 2002).
- ⁴⁵S. M. Malek, P. H. Poole, and I. Saika-Voivod, "Surface tension of supercooled water nanodroplets from computer simulations," *J. Chem. Phys.* **150**, 234507 (2019).
- ⁴⁶F. P. Buff, R. A. Lovett, and F. H. Stillinger Jr, "Interfacial density profile for fluids in the critical region," *Phys. Rev. Lett.* **15**, 621 (1965).
- ⁴⁷P. H. Poole, F. Sciortino, U. Essmann, and H. E. Stanley, "Phase behaviour of metastable water," *Nature* **360**, 324–328 (1992).
- ⁴⁸O. Mishima, "Polyamorphism in water," *Proc. Natl. Acad. Sci. U.S.A.* **86**, 165–175 (2010).